SUPPLEMENTARY INFORMATHION

Magnetoresistive Emulsion Analyzer

Gungun Lin[1,2], Larysa Baraban[3,*], Luyang Han[1], Daniil Karnaushenko[1,2], Denys Makarov[1], Gianaurelio Cuniberti[3,4], and Oliver G. Schmidt[1,2]

[1] Institute for Integrative Nanosciences, IFW Dresden, Helmholtzstr. 20, 01069 Dresden, Germany;
[2] Material Systems for Nanoelectronics, Chemnitz University of Technology, Reichenhainerstr. 70, 09107 Chemnitz, Germany;
[3] Max Bergmann Center of Biomaterials, Dresden University of Technology, Budapesterstr. 27, 01069 Dresden, Germany;
[4] Division of IT Convergence Engineering, POSTECH, Pohang, Korea
* Corresponding author: larysa.baraban@nano.tu-dresden.de

Supplementary Figure 1 | Study on the size and concentration dependency of emulsion droplets

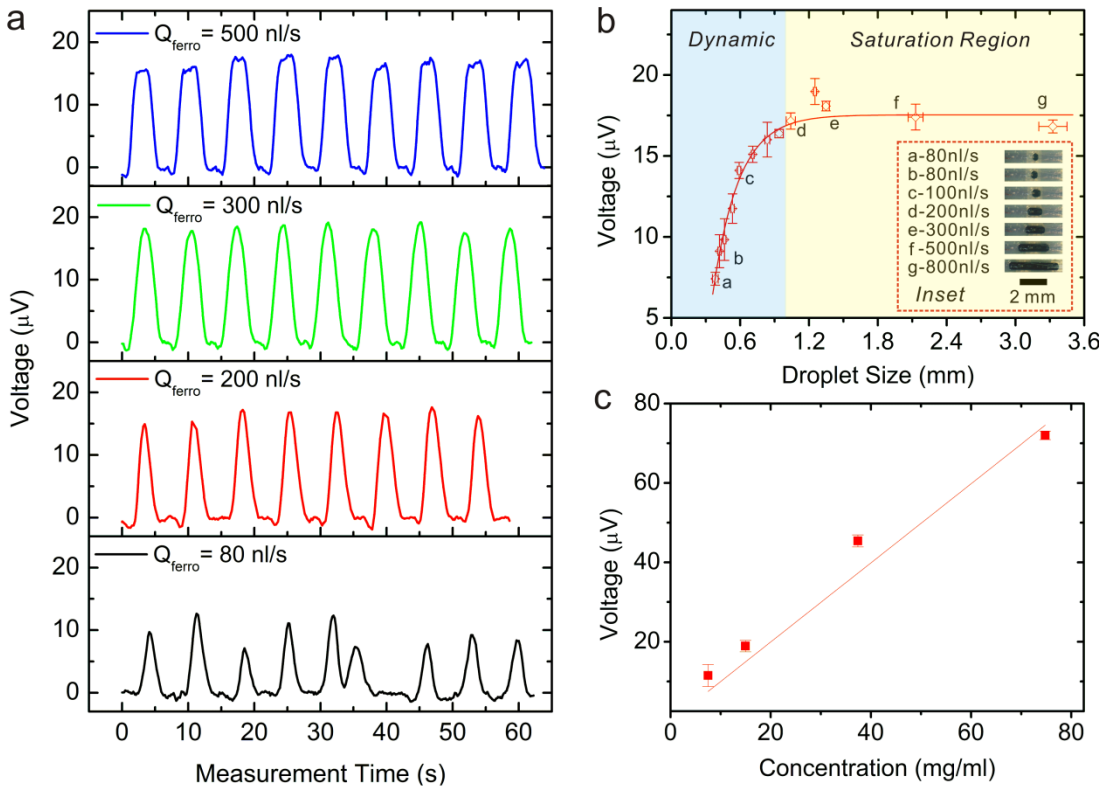

(a) Real time detection of ferrofluid emulsion droplets under various pulse flow conditions. The pulse amplitude of mineral oil was maintained constant at Q_{oil} = 500 nl/s, while that of ferrofluid was varied with Q_{ferro} = 80, 200, 300, 500 nl/s, respectively. (b) Dependence of the voltage change on the size of ferrofluid droplets with concentration of 15 mg/ml. The solid line is a guide to the eyes. The correlation was established by real time monitoring the ferrofluid droplets with an installed camera. The inset shows the corresponding ferrofluid droplets of different sizes produced under different flow conditions. (c) Dependence of voltage signal on the concentration of ferrofluid droplets under pulse flow conditions (Q_{oil} = 500 nl/s, Q_{ferro} = 300 nl/s). The linear relation still holds in the dynamic region as well due to the following reason: concentration of magnetic nanoparticles is proportional to the total magnetic moment of the droplet in the assumption that agglomeration is not present as is true for ferrofluids. In turn, magnetic stray fields of the droplets are proportional to the magnetic moment of the droplet. GMR sensor is detecting magnetic stray fields from the magnetic droplet. Therefore, strength of the sensor response will be proportional to the concentration of the ferrofluid in dynamic and saturated regime.

Supplementary Figure 2 | Histograms of the FWHM and standard deviations of the amplitude and FWHM for droplets with different volumes and concentrations

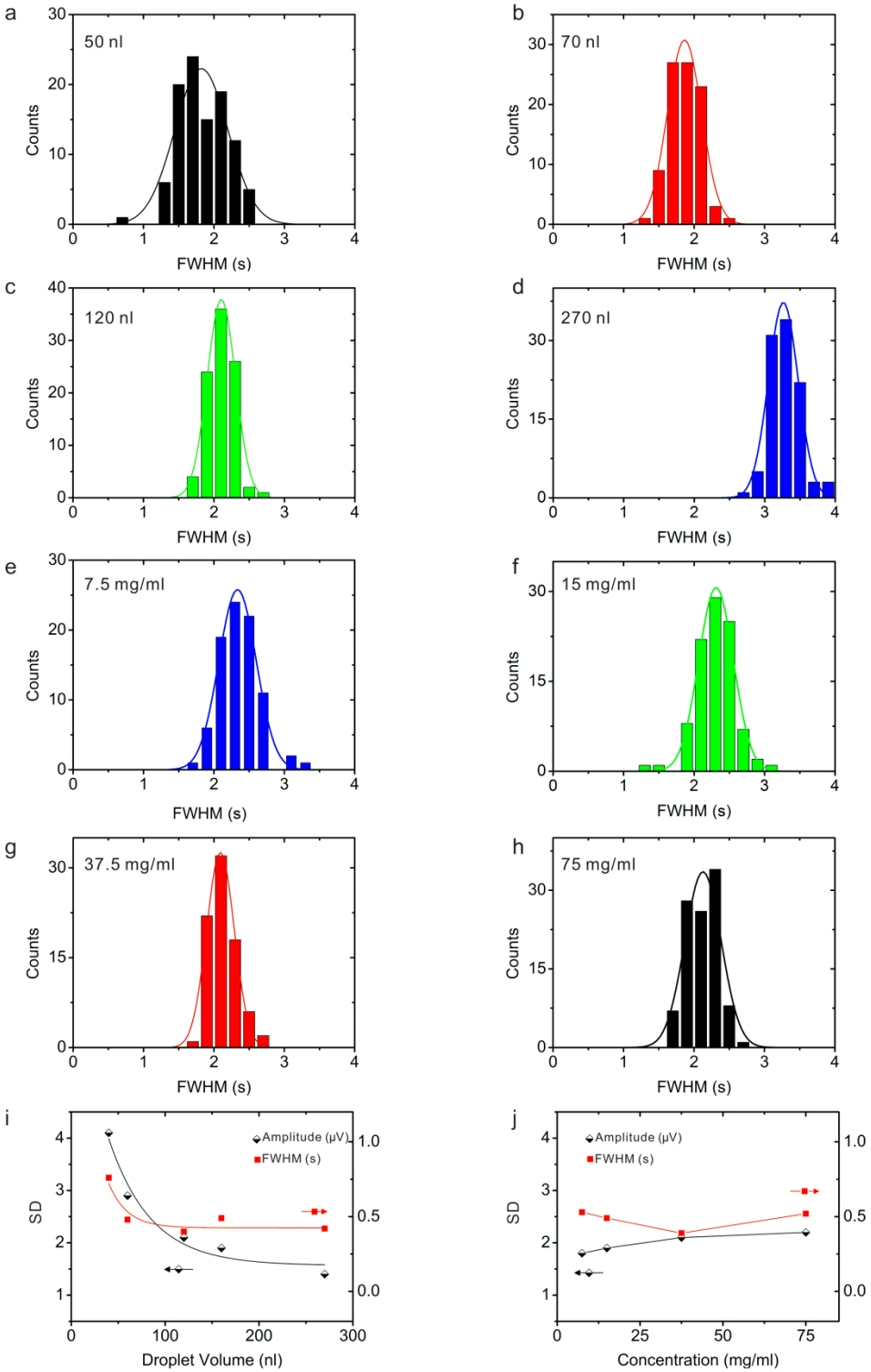

Histograms of the FWHM for ferrofluid droplets produced with different volumes (a-d) and concentrations (e-h). The standard deviations of the amplitude and FWHM derived from the Gaussian fit to the histograms for ferrofluid droplets with different volumes (i) and concentrations (j). Lines are guide to the eyes.

Supplementary Figure 3 | Dipole field simulation of detection peak patterns

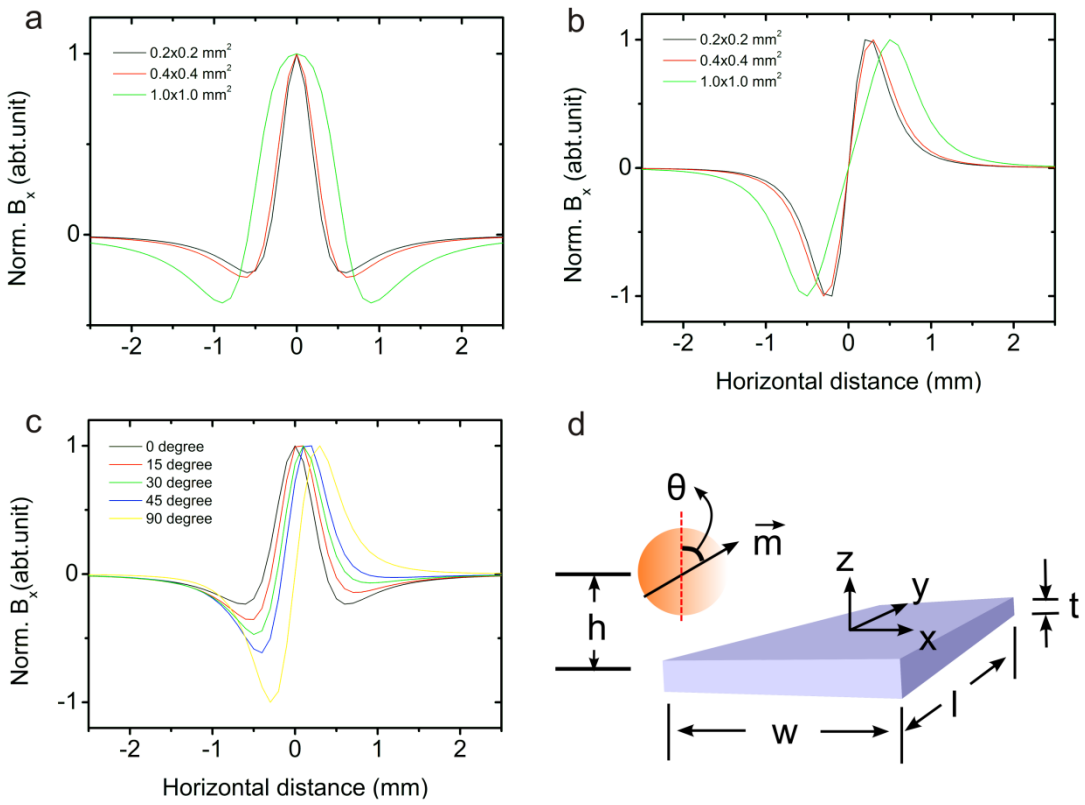

(a) The effective stray fields of the in-plane magnetized droplet against the horizontal distance (x) of the droplet from the GMR sensor for different sensor effective area (1.0×1.0 mm^2, 0.4×0.4 mm^2, and 0.2×0.2 mm^2). (b) The effective stray fields of the out-of-plane magnetized droplet against the position of the droplet from the GMR sensor for different sensor effective area. (c) The evolution of the effective magnetic stray fields against the position of the droplet magnetized along different orientations. The effective sensor area is taken as 0.4×0.4 mm^2. (d) The droplet is assumed to be of spherical shape, the size of which is taken to be equal to the inner diameter (ID) of the millifluidic channel (0.40 mm). The vertical distance (h) of the droplet from the sensor surface is 0.45 mm. The droplet has magnetic moment oriented in the x-z plane and with tilted angle of θ with respect to the z axis. The GMR sensor locates at the origin of coordinate system and in the x-y plane, which has width (W) and length (L).

Supplementary Figure 4 | Detection peaks for emulsion droplets with different orientation of magnetizations

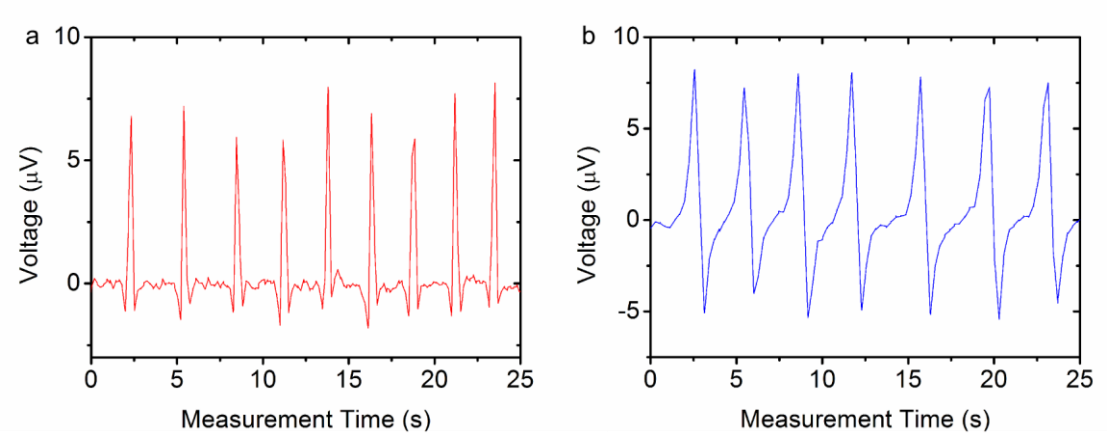

Real time detection results of ferrofluid emulsion droplets with magnetization of strong in-plane (a) and out-of-plane component (b). Droplets were produced under the following flow condition: Q_{ferro} = 5 nl/s and Q_{oil} = 200 nl/s.

Supplementary Figure 5 | Schematic description of the experimental setup

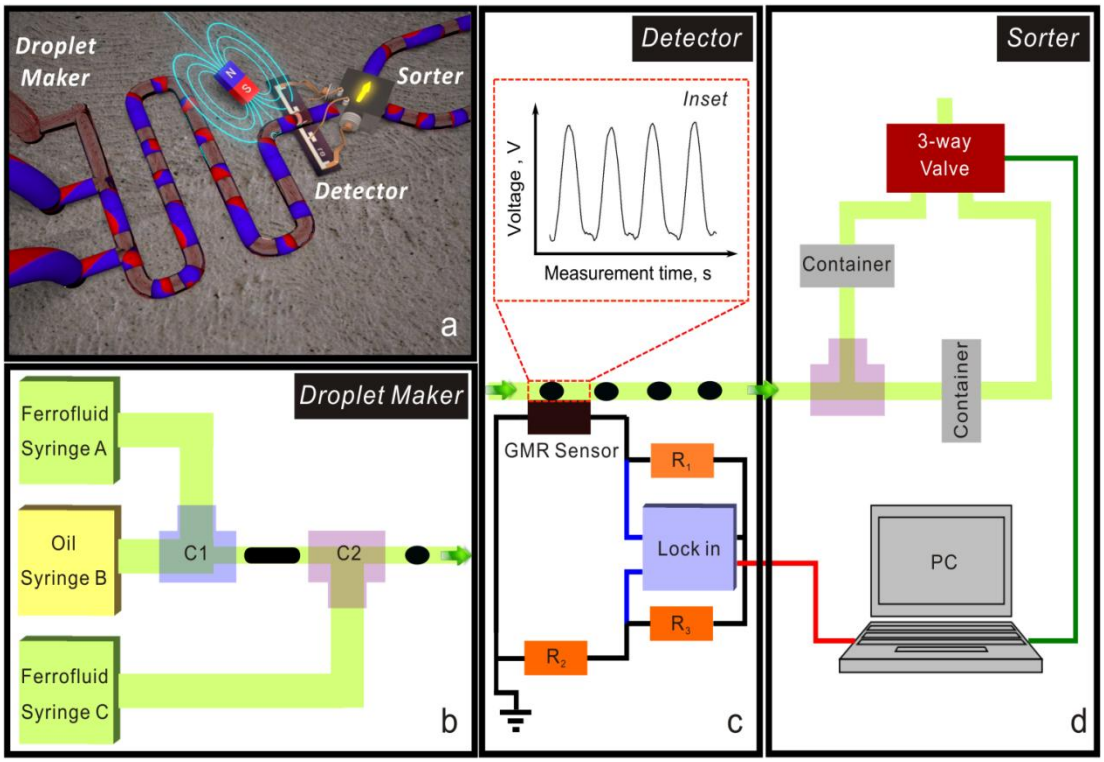

(a) Conceptional image of magnetoresistive emulsion analyzer for multiparametric analysis and sorting in millifluidics. (b-d) Schematics of the experimental setup. Droplet generation module (panel-b): This module is used to produce ferrofluid droplets under various flow conditions based on T-junction connectors. For the purpose of magnetic sorting, two T-junctions (C1 and C2) with different thru-hole diameters (C1: 0.5 mm, C2: 0.25 mm) are employed to produce trains of small ferrofluid droplets spaced by big ferrofluid droplets. Magnetic detection module (panel-c): GMR sensor implemented in the proximity of droplets flowing channel can detect the stray fields produced from the ferrofluid droplets and the voltage signal (blue lines) from the Wheatstone bridge is picked up and amplified by a lock-in amplifier. GMR-based sorting module (panel-d): The 3-way isolation valve is remotely controlled by the computer to divert the droplets into the corresponding channel. The containers are used to recycle the droplets and prevent the droplets from contaminating the valve.

Supplementary Figure 6 | An example of the flow profiles of oil and ferrofluids

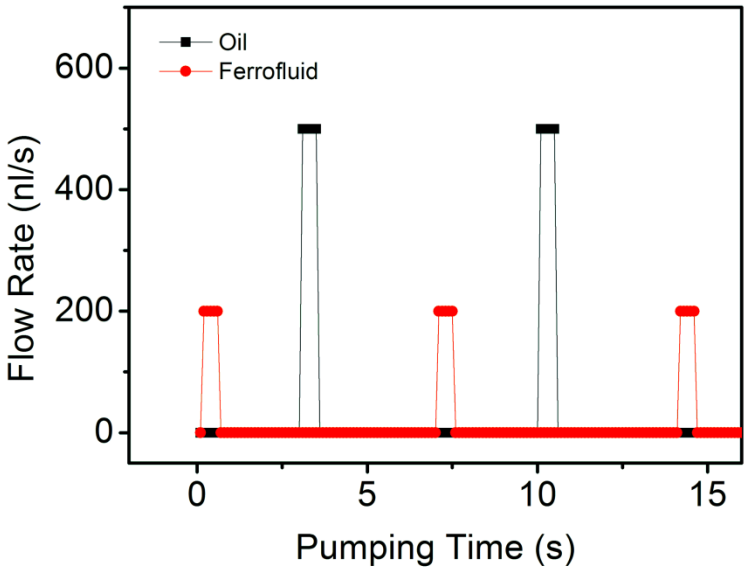

An example of pulse flow profiles of continuous phase (mineral oil) and disperse phase (ferrofluid) with Q_{oil} = 500 nl/s, Q_{ferro} = 200 nl/s. Oil and ferrofluid are pumped into the fluidic channel alternately in periodic pulses. Each pulse lasts for 500 ms, with 7s interval.

Supplementary Results

Size and Concentration Study

We assembled the droplet generation module as described below, sub-section **Supplementary Methods**. Droplets of different sizes and concentrations can be produced to study the device response to different sizes and concentrations of droplets. We next demonstrated the capability of the magnetoresistive emulsion analyzer to detect ferrofluid emulsion droplets. The real-time detection results of ferrofluid droplets with concentration of 15 mg/ml are summarized in **Supplementary Figure 1a**. Different sizes of droplets were produced under different flow conditions. An example of the flow profiles is shown in **Supplementary Figure 6.** The measured voltage shown **in Supplementary Figure 1a** is the differential voltage change of the Wheatstone bridge circuit as described in **Supplementary Methods**. We maintained the pulse amplitude of oil at constant value of 500 nl/s, while the pulse amplitude of ferrofluid was varied (Q_{ferro} = 80 nl/s, 200 nl/s, 300 nl/s, 500 nl/s), thus droplets of increasing sizes can be formed. As shown in **Supplementary Figure 1a**, each peak represents the detection event of single ferrofluid droplet. A gradual transition of the detection peak pattern (such as amplitude and width) is observed when the size of droplets increases. The real time measurement results show a clear dependence of signal voltage change on the pulse flow conditions, which indicates that *the GMR-based droplet analyzer is capable of nonvisual control of the droplet generation process*. At low flow rates of ferrofluid i.e. 80 nl/s, the detection events are represented by more irregular, less periodic peak pattern. This is mainly caused by too small droplets produced at the junction that have sizes slightly smaller than the inner diameter of the channel. The small droplets tend to flow with different speeds and to concentrate in the fluidic tube before they are pushed forward by the mineral oil, causing irregularities of the whole sequence. The phenomenon can be eliminated by raising the flow rate of ferrofluid, as shown by the following diagrams (200 nl/s and 300 nl/s). Detection peak patterns become more regular and uniform when the flow rate of ferrofluid is raised. Once the length of the ferrofluid droplets is larger than the width of the GMR sensor (about 1mm), saturation of the voltage change is observed, which is represented by the plateau in the detection peak.

We further performed the study of the dependence of voltage change on the size of droplets. We installed a video camera above the sensor; therefore, droplets crossing the sensor can be monitored in real time and correlated with the detected signal change. The dependence of the detected voltage change on the size of the ferrofluid droplets produced under various flow conditions is displayed in **Supplementary Figure 1b**. The evolution of the droplet size under different flow conditions are shown in **Supplementary Figure 1b, inset**. The volume of the ferrofluid droplets spans from about 20 nl to around 400 nl when the flow rate of ferrofluid is increased from 80 nl/s to 800 nl/s. It is shown that, the voltage change increases drastically with the increase of droplet size when the droplet is smaller than the size (1 mm) of the sensor, as denoted by the boundary between the regions that are marked blue and yellow. When the size of droplets exceeds the width of the sensor, the voltage change reaches a saturation value about 17.5 μV, which is ascribed to the fact that the GMR sensor only detects stray fields in its proximity. The dependence of the voltage change on the concentration of ferrofluids is displayed in **Supplementary Figure 1c**. We performed the measurement under the same flow condition (Q_{oil} = 500 nl/s, Q_{ferro} = 300 nl/s) which leads to an average droplet volume about 160 nl. The voltage change is observed to scale

almost with the concentration of ferrofluid.

Multiparametric analysis

The detection events of ferrofluid droplets are represented by the detected peaks (**Supplementary Fig. 1a**). Each peak can be characterized by its amplitude, the full-width at half maximum (FWHM), positive/negative amplitude ratio (PNR). These characteristics can serve as fingerprints for each ferrofluid droplet. For instance, the amplitude is related to the size and concentration of droplets, the FWHM contains the information about the speed and size of droplets, while the orientation of magnetization of the ferrofluid droplets is relevant to the PNR. These distinct features can be used to discriminate each labeled magnetic object. We performed the following experiments at a fixed flow conditions. Therefore, modifications of the FWHM are mainly attributed to the different size of droplets. Based on the previous studies, the size and concentration of ferrofluid droplets can be controlled and deterministically correlated to the derived voltage change.

We performed multiparametric analysis on the ferrofluid emulsion droplets. The amplitude and FWHM of the detection peak were derived by a Gaussian fit to the peak and taken for the established parametric analysis. Since the amplitude and FWHM are related to the droplet size and flowing speed, the distribution of the droplet size and amount of ferrofluids under fixed flow condition can be evaluated. FWHM is dependent not only on the size of droplets but also on their velocities. Therefore, the combined multiparametric analysis of the amplitude and FWHM can be used for the evaluation of the droplet size as well as the flow conditions. The multiparametric density plots for the ferrofluid droplets (with concentration of 15 mg/ml) with different volumes are summarized in **Figure 2a** (in the manuscript). The plots collect over about 100 droplets. The broad distribution of the FWHM and amplitude (**black cloud, Fig. 2a,** in the manuscript) is consistent with the real time detection results (**Supplementary Fig. 1a**). Also the corresponding fitted histogram displayed in **Figure 2c** (in the manuscript) indicates a clear polydispersity of droplet size. The droplet volume increases with the increase of flow rate of ferrofluids. The size of ferrofluid droplets is smaller than 1 mm for the flow rate of ferrofluid up to 200 nl/s. Thus the sensor is still working within the dynamic range as marked by the blue region in **Supplementary Figure 1b**. The amplitude of voltage change is sensitive to the change of droplet size. Thus, a narrow distribution of the data point cloud and the decrease standard deviation of the amplitude and FWHM in the fitted histograms (**Fig 2c**, in the manuscript) indicates a more uniform distribution of droplet size at larger volumes. The standard deviations are derived by a Gaussian fit to the histograms of amplitude and FWHM, respectively. The elliptical circles in **Figure 2a,b** in the manuscript are guide to the eyes. The elliptical circle is located at the center of the Gaussian fits to the histograms of the amplitude and FWHM, while the long and short axis of the elliptical circles take the half width values of the Gaussian fit to the amplitude and FWHM histograms. With droplet volume of 270 nl, the sensor is saturated. The variation of voltage change amplitude can reflect the concentration variation. However, in this case, the analysis shows that the standard deviation of amplitude is below 2 μV (see **Supplementary Fig. 2i**), which is smaller than the binning size of the histogram and close to the noise level (around 1.5μV). This indicates that concentration variation per droplet contributes to the change of amplitude to lesser extent in the experiments. The histogram of amplitude can clearly reflect the size distribution of droplets when the sensor is still working in the dynamic region. However, as mentioned, when the size of

droplets is larger than the sensor width, the sensor response is saturated with even larger size of droplets. Nonetheless, from the FWHM, the information of droplet size can still be extracted, which can be seen from the fact that the magnitude of FWHM increases as the droplet volume increases from 120 nl to 270 nl .We next performed the multiparametric analysis of droplets with different concentrations which were produced under the same flow condition (Q_{oil}= 500 nl/s, Q_{ferro} = 300 nl/s). The clouds of detection characteristics for droplets with different concentrations naturally fall into the same FWHM region (**Supplementary Fig. 2e-h**) indicating the consistent, homogeneous distribution of the droplet size for each specified concentration. The standard deviation of FWHM and amplitude for each specified concentrations levels off (**Supplementary Fig. 2j**), which indicates a relative consistent and homogenous droplets produced under the same flow conditions for each specified concentration. However, due to the scaling of voltage change with the magnetic moment, the center of the data point cloud is clearly shifted to higher voltage amplitudes for droplets with larger concentration of magnetic nanoparticles

GMR-based magnetic sorting

We refined the droplet generation module by using two T-junction connectors (**Supplementary Fig. 5a)** to realize ferrofluid droplet chains with small ferrofluid droplets evenly separated by larger droplets (**Supplementary Movie 1**). The shape of detection peaks comes from ferrofluid droplets which have magnetization with strong in-plane component. Detailed analysis of the detection peak pattern is performed based on a dipole field model (**Supplementary Fig. 3**). Ferrofluids with concentration of 75 mg/ml were used for the sorting experiments. The small droplets give an average voltage change about 7 μV, while the big droplets provide an average positive voltage change about 30 μV. The reduction of the voltage change amplitude might be due to the re-soldering of the electrical contact leading to the increase of contact resistance. During the sorting experiment, continuous flow conditions were employed with Q_{oil} = 200 nl/s and Q_{ferro} =5 nl/s for both junctions. The distance of the GMR sensor to the T-junction was 55 mm. By setting the threshold voltage value in between the voltage signal change coming from small and big droplets, the isolation valve was controlled to be only open when the big droplet crosses over the GMR sensor. Based on our sorting algorithm (**Supplementary Methods**), a delay time can be defined to delay the opening of the isolation valve when receiving the trigger. In this case, the valve was triggered right open for 13.5 s after 18.5 s delay and the big droplets can be successfully sorted out of the droplet chain into the desired channel (**Supplementary Movie 2**) as shown in **Figure d1, d2** (in the manuscript)**.**.

Simulation of detection peak pattern based on dipole field model

We employed Wheatstone bridge geometry to enhance the measuring sensitivity. The measured differential output voltage from the bridge can be expressed as:

$$\Delta V = V_s\left(\frac{R_s+\Delta R}{R_1+R_s+\Delta R} - \frac{R_2}{R_2+R_3}\right) \quad (1)$$

Here, V_s is the supplied constant voltage, R_s is the resistance of GMR sensor, R_1, R_2, and R_3 is the resistance of the trimmers (**Supplementary Fig. 5b**), respectively. ΔR is the change of the sensor resistance resulted from the stray fields from the ferrofluid droplets. Since ΔR is $<< R_1+R_s$, therefore, the above equation can be simplified as:

$$\Delta V = V_s\left(\frac{R_s+\Delta R}{R_1+R_s} - \frac{R_2}{R_2+R_3}\right) \quad (2)$$

As shown, the measured voltage change from the bridge ΔV scales with the change of the sensor resistance ΔR. Also, when the external magnetic field is small (due to the weak stray fields from the droplets), the change of the sensor resistance can be approximated to scale with the small change of external magnetic field. Therefore, the voltage change also scales with the change of external magnetic field under such situation.

The GMR sensor detects magnetic stray fields generated from the flowing ferrofluid emulsion droplets. To understand the origin of different detection peak patterns as shown in **Supplementary Figure 4** as well as to gain insights into the information that can be derived from the peak patterns, we analyzed the distribution of magnetic stray fields coming from the dynamically flowing ferrofluid emulsion droplets over the sensor surface. For the ease of calculation, several assumptions were made: (1) ferrofluid emulsion droplets are assumed to be spherical; (2) a ferrofluid droplet behaves as a single magnetic dipole moment, the stray fields of which is described by a dipole field model as given below:

$$\mathrm{B}(\mathbf{m},\mathbf{r}) = \frac{\mu_0}{4\pi}\left(\frac{3\mathbf{r}(\mathbf{m}\cdot\mathbf{r})}{\mathrm{r}^5} - \frac{\mathbf{m}}{\mathrm{r}^3}\right) \tag{3}$$

where $\mathrm{B}(\mathbf{m},\mathbf{r})$ being the magnetic flux density at the position described by the vector form $\mathbf{r}$, μ_0 being the permeability, and $\mathbf{m}$ being the magnetic dipole moment.

Considering the exchange coupling and magnetic anisotropy within the sensor film, as well as the fast decay of stray fields over distance, an effective sensor sensing region is defined so that the stray fields only act on this region, beyond which the stray fields of ferrofluid droplets do not contribute to the change to sensor resistance. The resultant effective stray fields from ferrofluid droplets can be calculated from:

$$\mathrm{B_s}(\mathbf{m},\mathbf{r}) = \iiint \left[\frac{\mu_0}{4\pi\mathrm{lwt}}\left(\frac{3\mathbf{r}(\mathbf{m}\cdot\mathbf{r})}{\mathrm{r}^5} - \frac{\mathbf{m}}{\mathrm{r}^3}\right)\right] \mathrm{dxdydz} \tag{4}$$

Here $\mathrm{B_s}(\mathbf{m},\mathbf{r})$ is the effective stray fields derived from the integral of the averaged stray fields over the sensor volume (l×w×t) that contributes to the change of sensor resistance, w, l, t is the width, length and the thickness of the effective sensing region.

In the experiments, a permanent magnet was employed to magnetize ferrofluid droplets and to bias the sensor. Due to the variation in the space distribution of stray fields from the permanent magnet during the adjustment, the magnetization of the ferrofluid droplet might be oriented along certain direction after the adjustment of the permanent magnet. Thus, the pattern of the detection peak pattern can be varied (**Supplementary Fig. 4**) according to the arrangement of the magnet. Furthermore, as the GMR sensor is only sensitive to the in-plane magnetic fields, only the in-plane component of the stray fields from a ferrofluid droplet is taken into account.

For the calculation, we neglected vertical differences in the sensor volume (l×w×t), because the thickness of the GMR sensor (around 100 nm) is much smaller than the distance of the droplet from the sensor surface (0.45 mm). Thus, the effective stray fields were calculated by averaging the stray fields over an effective sensing area (l×w), and the size of the ferrofluid droplet was chosen to be 0.40 mm, which equals the inner diameter of the millifluidic channel. As shown in **Supplementary Figure 3d**, the origin of the coordinate system locates in the center of the effective sensing area of the sensor. The vertical distance (h) of the droplet to the sensor is 0.45 mm. To study the dynamic response of GMR sensor to the flowing droplets, the effective stray fields from the droplet was calculated with respect to the horizontal distance of the droplet from the GMR sensor.

Supplementary Figure 4 summarizes several calculated examples of the effective stray field pattern from ferrofluid droplets with in-plane (a) or out of plane (b) magnetization. Different sensor effective sensing areas were chosen to simulate the influence of sensor sensing area to the detection peak pattern. Therefore, the origin of the shape of the detection peak pattern in **Supplementary Figure 1a** (80 nl/s) and **Supplementary Figure 4a**, as well as in **Supplementary Figure 4b** can be understood from the simulations as shown in **Supplementary Figure 3a,b**, respectively. The detection peak of an in-plane magnetized ferrofluid droplet is characterized with maximum stray fields when the droplet is crossing the center of the sensor; while for the out-of-plane magnetized droplet, it shows a bipolar shape pattern. This further points out that the detection peak patterns from ferrofluid droplets can be used as 'fingerprints' for individual droplet. The effective sensing area of the sensor may influence the detection peak pattern as well. The ratio of the stray field maximum and minimum is increasing with the decrease of effective sensing area of the sensor, which takes effect particularly for droplets with the in-plane magnetization. The tilting of magnetization of ferrofluid droplets from a pure in-plane or out-of-plane direction results in an asymmetric stray field pattern, as shown in **Supplementary Figure 3c**.

Considering detection peak patterns from ferrofluid droplets produced under flow rate of ferrofluid of 80 nl/s as displayed in **Supplementary Figure 1a** as well as those in the sorting experiment (**Fig. 1c**, in the manuscript), the droplets formed at the T-junction can be approximated as spherical shape. Thus the origin of slightly asymmetric detection peaks can be ascribed to the slightly tilted magnetization of ferrofluid droplets with strong in-plane component.

With the increase of flow rate of ferrofluids, the shape of droplets evolves from spheres to plugs. Earlier simulations[1] on the detection peak patterns of ferrofluid plugs by a GMR sensor based on AMPERES software showed a local minimum of stray fields located below the center of a ferrofluid plug, which is consistent with the detection peak patterns of ferrofluid plugs produced at higher flow rate (500 nl/s) of ferrofluid in our measurements. The small drop of the voltage change at the detection peak plateau (500 nl/s, **Supplementary Fig. 1a**) is indicative of this mechanism.

Supplementary Discussion

Although quite a lot of cytometric tools based on optical means[2-4] has been reported by many research groups, there is still no a GMR-based cytometric device that is readily available to perform full functionalities. The present research work describes the first method that is able to count, analyze, and sort magnetic emulsions that have vast applicability, i.e. in biomedicine as magnetic labels, as contrast agent for MRI, or as a tool for separation of biochemical species and therapies, or even used in pharmaceutical applications for drug design and screening. Combining droplet-based fluidic technology, we first demonstrated the counting ability of the GMR-based emulsion analyzer, and studied the size and concentration dependencies of the device response. The analyzer was very sensitive to the size of magnetic emulsion droplets when the size of droplets is smaller than the width of sensor, which renders the sensor a functionality to sort emulsions by size. Also the study on the concentration of emulsion droplets reveals that a quantitative determination of the magnetic content as carried by the emulsion droplet is possible. This opens up promising perspectives for drug design where the doses of the magnetically-tagged drugs per droplet can be determined. The characterization of the performance of the analyzer with

respect to the size and concentration of emulsion droplets indicates that drug screening with this method is possible which can be based on either the size or the concentration of emulsion droplets, e.g. liposomes, which are used to label the drugs.

The multiparametric analysis on ferrofluid emulsion droplets, to our knowledge, is the first method so far that allows the analysis of ferrofluid emulsion droplet in terms of size and magnetic concentrations, which, as pointed out, can be used to analyze the magnetically-tagged drugs in biomedicine or simply be used as a tool for evaluating the emulsification procedure. In contrast to the optical cytometric approach using forward and side scattered light as parameters to analyze different cell types, our method employs the amplitude and FWHM which serve as useful parameters to analyze the size and concentration of the emulsions that can be potentially carrying various biospecies. Therefore, the populations of different types of emulsions can be studied. Also multiplex assays relying on various concentrations of emulsion droplets are feasible.

Apart from counting and analysis, sorting of emulsion droplets were demonstrated with the GMR-based emulsion analyzer. The sorting functionality enables the tool to sort or purify biochemical species of specific property. We believe that the combination of counting, analysis and sorting of ferrofluid emulsions will advance the development of drug design and screening. Also we anticipate that the application of magnetoresistive emulsion analyzer may bring perspectives in modern bioassays and clinical diagnostics.

Supplementary Methods

Droplet generation module

The ferrofluid droplets are formed on a T-junction connector, where aqueous solution of ferrofluid (water-based ferrofluid, Ferrotec EMG Series 700) is dispersed in the mineral oil phase (mineral oil, Sigma-Aldrich M8410). The droplet generator module (**Supplementary Fig. 5a**) was assembled from several components: the pulse free syringe pumps (neMESYS, Cetoni) for fluid injection; the T-junction for droplet formation; interconnections, i.e. flangeless fittings (standard ¼–28 thread), syringes (1000 Series, Hamilton, syringe volume: 1.0 ml and 2.5 ml); flow circuits that were realized with polytetrafluoroethylene (PTFE) tubing with outer diameter (OD) of 0.9 mm and inner diameter (ID) of 0.4 mm. We used the pulse flow approach to generate droplets of different size for multiparametric analysis. An example of the flow profiles of two immiscible phases are displayed in **Supplementary Figure 6**. The period of flow pulses is 7 s, while each flow pulse lasts for 500 ms.

Magnetic detection module

The layer stack of the GMR multilayers was: [Py (1.5 nm)/Cu (2.2 nm)]$_{30}$/Py (1.5 nm), which was prepared by magnetron sputtering technique under high vacuum condition (base pressure: 2.5×10^{-7} mbar). Ar was employed as the sputter gas, the pressure of which was controlled at 1.6×10^{-3} mbar. Before depositing the layer stack, a thermally oxidized silicon wafer with 1000 nm SiO_x layer was patterned into rectangular stripe (width: 1 mm, length: 16 mm) by standard optical lithography using image reversal technique. The optical lithography was performed in the clean room with standard class 100 conditions. Firstly, the silicon substrate covered with 1 μm oxide was spin coated with TI-Prime (MicroChem Corp.) at 4500 rpm for 35 s, followed by a baking at 120 °C for 3 min. After that, negative photoresist (AZ5214E) was spin coated onto the substrate at 4500

rpm for 35 s, which was subsequently baked at 90 °C for 4 min. Then the sample was exposed with the stripe pattern using MA56 mask (Karl Süss) aligner for 2 s, and post-baked at 120 °C for 2 min. Subsequently, the sample was exposed without mask for 30 s to realize image reversal. At the end, the sample was developed by AZ726MIF developer (Microchem) for 1 min, and rinsed by DI water.

Magneto-electrical characterization was performed based on conventional 4-point method. The GMR sensor was placed in between pole shoes of the electromagnets, where uniform in plane magnetic field was cycled between ±25 mT and the sensor resistance was recorded. The GMR sensor is a proximity sensor, which responses to local magnetic stray fields from the objects. Therefore, a strategy is taken to enhance the magnetic stray fields to be detected. As the ferrofluid (EMG 700, Ferrotec) employed for present study is a suspension of magnetic colloidal nanoparticles in water, it does not retain remanence without applying external magnetic field. Thus, an external field should be applied to achieve a net magnetization of the ferrofluid. In addition, the external magnetic field can be simultaneously used to bias the sensor to the sensitive region. Based on the above considerations, a permanent magnet (AlNiCo 500, type A1560, IBSMagnet, length: 60 mm, diameter: 15 mm) was placed below the GMR sensor which was mounted on a movable stage. With adjustment of the position of the permanent magnet, the sensor was biased to the most sensitive region and the stray fields from the magnetized ferrofluid were sufficient to be detected by the GMR sensor. Further, the tubing was placed in close contact to the sensor surface to enhance the stray fields that can be detected.

The GMR sensor was soldered and connected with 3 other trimmers (Bourns, 3006P-1-102LFto realize a Wheatstone bridge geometry (**Supplementary Fig. 5c**). By balancing the bridge, the background voltage from the bridge can be minimized to enhance the measuring sensitivity. The lock-in amplifier (SRS830) was used to amplify the signal and reduce the noise. The whole bridge circuit was powered also by lock-in with constant ac voltage of 0.800 V. The modulation frequency was 1 kHz and the time constant was 10 ms. The sensitivity of lock-in was set at 500 µV with a resolution of 10 nV, which was sufficient to resolve the voltage signal. The analog output from the lock-in was sampled at 512 Hz and transferred to the computer. Affiliated to the sensing platform a digital camera (DNT Microdigit) was installed which was used to monitor the flowing droplets. Videos and pictures of flowing droplets can be correlated with the voltage signals obtained with the GMR sensor.

GMR-based sorting module

The droplet generation module was refined to form a train of droplets of multiple sizes for the sorting (**Supplementary Fig. 5a**). The module was composed of two T-junctions (C1and C2) with different thru-hole diameters (C1: 0.5 mm, C2: 0.25 mm). Due to the differences in the size of thru-hole diameter, droplets of distinct size can be produced at these two junctions. Big droplets were formed in the junction C1 using syringe A, while smaller droplets were injected into the same fluidic channel through the junction C2 through syringe C. Such fluidic assembly resulted in the sequence of the droplets with alternating size, which was further used for sorting experiments. The sorting part was composed of a T-junction (**Supplementary Fig. 5d**, thru-hole diameter: 0.25 mm) flanked by two separate fluidic channels that were connected to a solenoid 3-way isolation valve (Amico Scientific) as mentioned before. The 3-way valve was with one-way open and one-way closed without supplying power. The switching of the valve was controlled by an

external power source (Agilent Precision Source/Measurement Units B2902A) with working voltage of 24 V. In the sorting experiment, applied voltage of 20 V with compliance of 0.5 mA was sufficient to switch on the valve. The algorithm of magnetic sorting is described as follows: ferrofluid droplets of different size are detected by the GMR-based millifluidic droplet detector. The electrical signal from the detector is analyzed and compared to the threshold value. A threshold voltage is defined to trigger the on/off performance of the solenoid 3-way isolation valve installed behind the sensor, so as to allow the droplets of interest to be sorted into the corresponding channel. A hold-time and delay-time are set to determine how long the valve to be kept open and when the opening of the valve will be delayed after receiving a signal trigger from the GMR sensor. This feature is crucial when the spacing between droplets is smaller than the distance between the GMR sensor and the sorting junction.

References

1. Pekas, N., Porter, M. D., Tondra, M., Popple, A. & Jander, A. Giant magnetoresistance monitoring of magnetic picodroplets in an integrated microfluidic system. *Applied Physics Letters* **85**, 4783 (2004).
2. Krutzik, P. O. & Nolan, G. P. Fluorescent cell barcoding in flow cytometry allows high-throughput drug screening and signaling profiling. *Nature methods* **3**, 361–8 (2006).
3. McKenna, B. K., Evans, J. G., Cheung, M. C. & Ehrlich, D. J. A parallel microfluidic flow cytometer for high-content screening. *Nature methods* **8**, 401–3 (2011).
4. Kapoor, V. *et al.* New lasers for flow cytometry: filling the gaps. *Nature methods* **4**, 678–9 (2007).